Role of Conserved Active Site Residues in Catalysis by Phospholipase B1 from *Cryptococcus neoformans*†

Peter M. Jones,‡ Kylie M. Turner,§ Julianne T. Djordjevic,§ Tania C. Sorrell,§ Lesley C. Wright,§ and Anthony M. George*,‡

Department of Medical and Molecular Biosciences, University of Technology Sydney, P.O. Box 123, Broadway, NSW 2007, Australia, and Centre for Infectious Diseases and Microbiology, Westmead Millennium Institute and University of Sydney, ICPMR Building, Westmead Hospital, Westmead, NSW 2145, Australia

Received May 17, 2007; Revised Manuscript Received June 18, 2007

ABSTRACT: Phospholipase B1 (PLB1), secreted by the pathogenic yeast *Cryptococcus neoformans*, has an established role in virulence. Although the mechanism of its phospholipase B, lysophospholipase, and lysophospholipase transacylase activities is unknown, it possesses lipase, subtilisin protease aspartate, and phospholipase motifs containing putative catalytic residues S146, D392, and R108, respectively, conserved in fungal PLBs and essential for human cytosolic phospholipase A_2 ($cPLA_2$) catalysis. To determine the role of these residues in PLB1 catalysis, each was substituted with alanine, and the mutant cDNAs were expressed in *Saccharomyces cerevisiae*. The mutant PLB1s were deficient in all three enzymatic activities. As the active site structure of PLB1 is unknown, a homology model was developed, based on the X-ray structure of the $cPLA_2$ catalytic domain. This shows that the two proteins share a closely related fold, with the three catalytic residues located in identical positions as part of a single active site, with S146 and D392 forming a catalytic dyad. The model suggests that PLB1 lacks the "lid" region which occludes the $cPLA_2$ active site and provides a mechanism of interfacial activation. In silico substrate docking studies with $cPLA_2$ reveal the binding mode of the lipid headgroup, confirming the catalytic dyad mechanism for the cleavage of the *sn*-2 ester bond within one of two separate binding tracts for the lipid acyl chains. Residues specific for binding arachidonic and palmitic acids, preferred substrates for $cPLA_2$ and PLB1, respectively, are identified. These results provide an explanation for differences in substrate specificity between lipases sharing the $cPLA_2$ catalytic domain fold and for the differential effect of inhibitors on PLB1 enzymatic activities.

Cryptococcal phospholipase B1 (PLB1)[1] is a multifunctional enzyme containing phospholipase B (PLB), lysophospholipase (LPL), and lysophospholipase transacylase (LPTA) activities (*1*). Although it is secreted, it also associates with membranes and the cell wall, presumably via a glycosylphosphatidylinositol (GPI) anchor (*2*). PLB activity catalyzes the simultaneous deacylation of glycerophospholipids at both *sn*-1 and *sn*-2 positions, LPL activity, the removal of a single acyl chain from a lysophospholipid, and LPTA activity, the transfer of an acyl chain from one lysophospholipid to another, forming a diacylphospholipid. Using animal and cell culture models of cryptococcosis, PLB1 has been shown to facilitate cryptococcal adherence to lung epithelium, establishment of interstitial lung infection, survival and replication of cryptococci within macrophages, and cryptococcal dissemination from the lung via lymphatics and blood (*3*−*5*).

Despite the importance of PLB1 in fungal virulence, no structural information is available, and nothing is known of the amino acid residues involved in the mechanism of PLB1 catalysis. However, PLB1 contains similar catalytic motifs to the mammalian cytosolic phospholipase A_2 enzyme $cPLA_2\alpha$ (PLA2G4A), namely, lipase (GXSXG), subtilisin protease aspartate (IXVVDSGLXXXN), and putative phospholipase (SGGGXRAM) motifs. The underlined S228, D549, and R200 residues have a role in $cPLA_2$ catalysis (*6*, *7*) and are conserved in $cPLA_2$ from six mammalian species (*7*) and in all fungal PLB enzymes (except *Schizosaccharomyces pombe*) (*4*, *8*−*16*). The $cPLA_2$ residues are analogous to S146, D392, and R108 in cryptococcal PLB1. In $cPLA_2$, S228 is thought to function as a nucleophile in the catalytic center, allowing formation of an enzyme-acyl intermediate (*6*, *17*), while D549 acts as a general base, activating S228 (*18*). R200 is not directly involved in catalysis but may stabilize the substrate phospholipid headgroup (*18*).

† This work was supported by Grants 211040 and 352354 (to J.T.D., T.C.S., and L.C.W.) from the National Health and Medical Research Council, the Ann Woolcock Biomedical Postgraduate Research Scholarship (to K.M.T.) from Community Health and Tuberculosis Australia, a Millennium Foundation Stipend Enhancement Grant (to K.M.T.), and an Australian Wool Innovation Fellowship and Australian Partnership for Advanced Computing Grant (to P.M.J.).

* To whom correspondence should be addressed. Phone: (612) 9514-4158. Fax: (612) 9514-8206. E-mail: tony.george@uts.edu.au.

‡ University of Technology Sydney.

§ Westmead Millennium Institute and University of Sydney.

[1] Abbreviations: $cPLA_2$, human cytosolic phospholipase A_2; LPL, lysophospholipase; LPTA, lysophospholipase transacylase; PLB, phospholipase activity; PLB1, phospholipase B protein; MD, molecular dynamics.

10.1021/bi7009508 CCC: $37.00
Published on Web 08/09/2007

$cPLA_2$ has a preference for arachidonic acid in the *sn*-2 position and only removes this chain (*18*), whereas PLB1 prefers either palmitoyl or oleoyl fatty acid chains in both the *sn*-1 and *sn*-2 positions and can remove both chains via the PLB activity (*1*). Previous studies have demonstrated that several agents [a PLB1 peptide antibody, carnitine, palmitoylcarnitine, *N*-ethylmaleimide, 5,5′-dithiobis(2-nitrobenzoic acid), dioctadecyldimethylammonium bromide, 1,12-bis-(tributylphosphonium)docecane dibromide, Triton X-100, and alexidine dihydrochloride] differentially inhibit either the LPL/LPTA or the PLB activities of secreted cryptococcal PLB1 (*1*, *3*, *19*, *20*), suggesting that PLB1 contains two active sites.

In this study, site-directed mutagenesis was used to investigate the roles of S146, D392, and R108 in catalysis of cell-associated and secreted PLB1. In the absence of PLB1 structural data, we constructed a homology model of PLB1 using the X-ray structure of the human $cPLA_2$ catalytic domain as a template. The stability of this model in molecular dynamics (MD) simulations suggests that PLB1 shares the same core fold and positioning of the catalytic residues within the active site groove as the $cPLA_2$ catalytic domain. The model also suggests an alternative role for the "lid" region of the cap domain to that involving interfacial activation at the membrane. In silico substrate-docking studies with $cPLA_2$ were also performed to identify regions and specific residues involved in fatty acyl chain binding, in order to explain differences in substrate specificity between lipases sharing the $cPLA_2$ catalytic domain fold, as well as the differential effect of inhibitors on the various enzymatic activities of PLB1.

EXPERIMENTAL PROCEDURES

Reagents. The Gene-tailor site-directed mutagenesis kit, platinum Taq DNA polymerase, and the anti-express antibody were obtained from Invitrogen (Mulgrave, VIC, Australia). ECL reagents, X-ray film, 1,2-di[1-^{14}C]palmitoylphosphatidylcholine, and 1-[1-^{14}C]palmitoyllysophosphatidylcholine were from Amersham Biosciences (Castle Hill, Australia). Carrier lipids dipalmitoylphosphatidylcholine and 1-palmitoyllysophosphatidylcholine, and *Trichoderma harzianum* (L1412) β-glucanase, were from Sigma (Castle Hill, Australia).

Strains and Plasmids. *Saccharomyces cerevisiae* strain JK93Dα CnPLB1 expressing PLB1 cDNA from *Cryptococcus neoformans* regulated by a galactose-inducible promoter from pYES2 and the expression vector pYES2:CnPLB1 were used as described (*2*). Strains were grown in uracil-deficient (URA^-) medium (*21*).

Preparation of PLB1 Mutants and Lysates. PLB1 mutants were prepared by site-directed mutagenesis using pYES2:CnPLB1 as template as described (*21*). Mutagenic primers for the putative active site residues were as follows: primer 1, for R108A (5′-TTG TCC GGC GGT GGT TAC GCT GCA ATG CTT A-3′); primer 2, for S146A (5′-TAA GCT ACT GGG CTG GTC TGG CCG GTG GGA GTT-3′); primer 3, for D392A (5′-TCA CTT ACA TCA CCC TCG TCG CTG CCG GAG AAA-3′). The underlined residues indicate the mutations, which were confirmed by DNA sequencing. Mutant cDNAs were used to transform *S. cerevisiae* strain JK93Dα. The altered PLB1 enzymes were designated PLB1(R108A), PLB1(S146A), and PLB1(D392A). *S. cerevisiae* lysates expressing wild-type and mutant PLB1 were prepared as described (*21*).

Subcellular Fractionation. This was performed as described (*21*). Briefly, wild-type and mutant PLB1 were induced in *S. cerevisiae* by incubation in medium containing galactose for 23 h. Cells were harvested by centrifugation, resuspended in secretion buffer containing 10 mM imidazole, 2 mM $CaCl_2$, 2 mM $MgCl_2$, and 56 mM galactose, made up in isotonic saline, pH 5.5, and allowed to secrete for 16 h at 30 °C. The cell-free supernatants (secretions) were collected by centrifugation. The cell pellets were homogenized and centrifuged to yield the 14K cytosol/membrane (CM) fractions (supernatants) and the 14K insoluble fractions (pellets). The 14K insoluble fractions were digested with β-1,3-glucanase (*T. harziarum*; 19 mg/mL in IAB buffer, pH 5.5) for 2 h at 37 °C to release cell wall-associated proteins (termed the "cell wall" fraction).

Western Blotting. Proteins in cell lysates were separated on 4−12% Bis-Tris gradient gels (Novex, Invitrogen) and subjected to Western blotting with the anti-PLB1 peptide antibody or the anti-Pma1p antibody as described (*2*, *21*). The secondary antibody was donkey anti-goat conjugated to HRP (Santa Cruz Biotechnology).

PLB1 Enzyme Assays and Protein Estimations. PLB1 enzyme assays were conducted as described in ref *1* under optimized conditions (*21*). Total protein content in all fractions was determined using the BCA protein assay kit and the Compat-Able protein assay preparation reagent set (Pierce Biotechnology), with BSA as standards. Statistics were calculated using GraphPad Instat version 3. The test used and the *P* values obtained are indicated in the table and figure legends. *P* values <0.05 were considered significant.

Homology Modeling and MD Simulations. Alignments were generated using CLUSTAL W (*22*). Homology models were generated using MODELLER 8v1 (*23*). The PHD algorithm was used for secondary structure and solvent accessibility prediction (*24*). Molecular dynamics simulations were performed using NAMD2.5 (*25*) and the CHARMM27 force field for protein and ligands (*26*), along with the TIP3P model for water (*27*). The SHAKE algorithm was used to constrain the bonds containing hydrogens to their equilibrium length (*28*). A cutoff of 11 Å (switching function starting at 9.5 Å) for van der Waals interactions and real space electrostatic interactions was assumed. Periodic boundary conditions were used, and distances between periodic images of the protein were 20 Å. The particle-mesh Ewald method (*29*) was used to compute long-range electrostatic forces. The density of grid points for particle-mesh Ewald was approximately $1/Å^3$. An integration time step of 1.5 fs was used, permitting a multiple time-stepping algorithm (*30*) to be employed in which interactions involving covalent bonds and short-range nonbonded interactions were computed every time step, and long-range electrostatic forces were computed every two time steps. Langevin dynamics was utilized to keep a constant temperature of 310 K in all simulations. Constant pressure simulations at 1 atm were conducted using the hybrid Nose'-Hoover Langevin piston method with a decay period of 100 fs and a damping time scale of 50 fs.

The protein was placed in a box of equilibrated water molecules, and sodium ions were added randomly to the

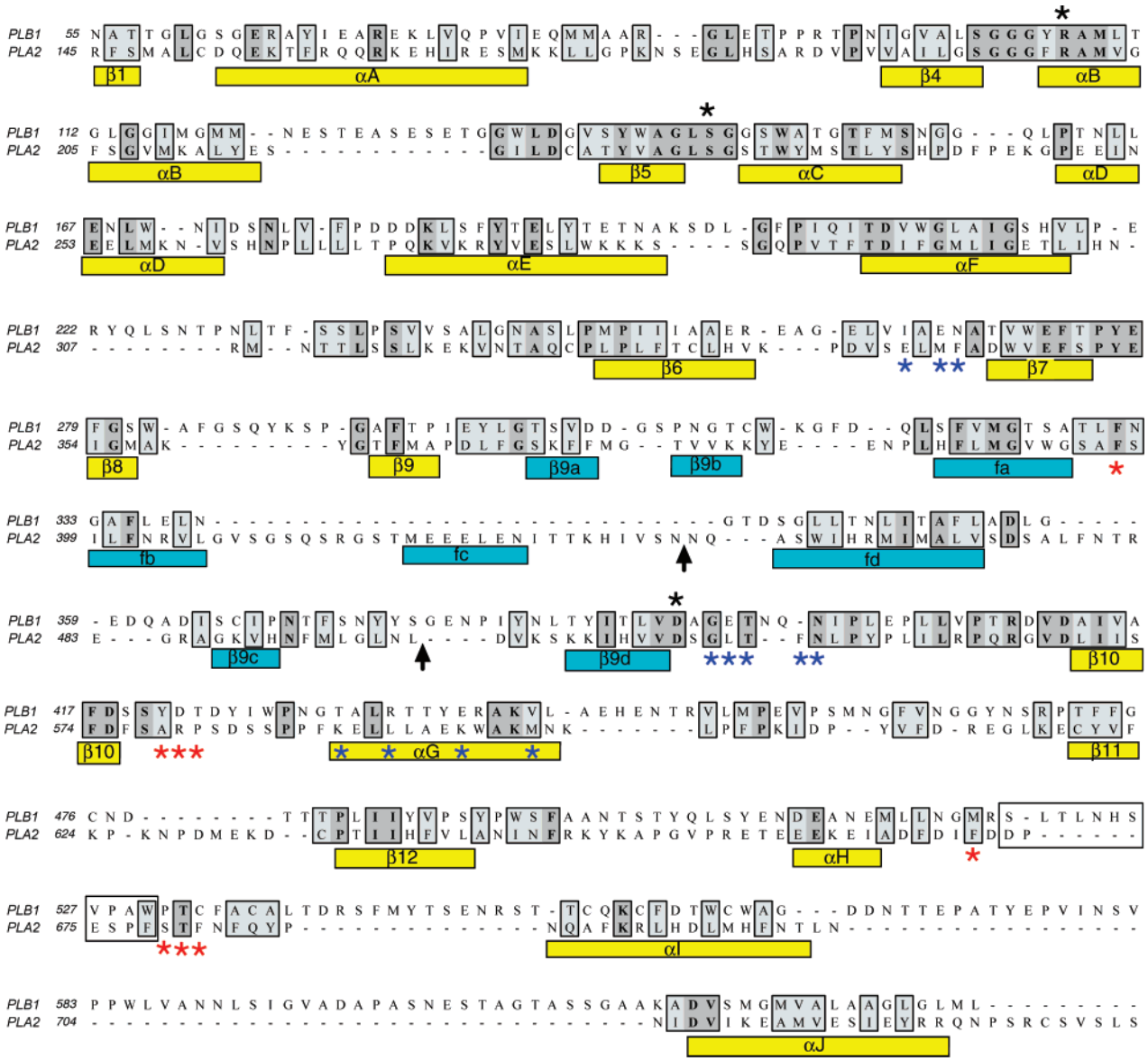

FIGURE 1: Manually adjusted CLUSTAL W alignment of PLB1 and the cPLA$_2$ catalytic domain used in the homology modeling of PLB1. Amino acid sequence homology between the two proteins is indicated by the gray-filled boxes (17% identity). Secondary structural elements in cPLA$_2$ are indicated by rectangles labeled according to ref *34* and colored yellow for core domain residues and cyan for cap domain residues. PLB1 residues mutated in this study are indicated by black asterisks. Residues which contact the arachidonoyl chain (and the palmitoyl chain) in the docking study are indicated with red and blue asterisks, respectively. A loop region between cPLA$_2$ residues 673 and 678 which may also be involved in substrate binding is indicated by an unfilled box. Arrows indicate the start of discontinuities in the cPLA$_2$ sequence between N432 to N460 and L498 to D539.

system to maintain electrical neutrality. The solvated starting structure was minimized using conjugate gradient minimization to a 0.5 kcal/(mol·Å) root mean square (rms) gradient with all protein heavy atoms fixed. Water molecules, counterions, and protein hydrogens were then further minimized during a 24 ps molecular dynamics run at 358 K, in which all protein heavy atoms were again fixed. This starting model was then minimized to a 0.5 kcal/(mol·Å) rms gradient with harmonic positional constraints using a 100 kcal/(mol·Å^2) force constant on the Cα atoms of the secondary structural elements (*β*-strands and α-helices), indicated in Figure 1. The constraints were gradually removed by subsequent minimizations to a 0.1 kcal/(mol·Å) rms gradient, scaling the initial force constants by factors of 0.5, 0.15, 0.05, and 0. The minimized structure was then heated from 60 to 310 K in steps of 25 K using velocity reassignment during an 18 ps MD run. The equilibrated system was then simulated without restraints for 2 ns.

Ligand Docking. Ligand docking was performed using DOCK version 6 available at http://dock.compbio.ucsf.edu/. Protein and ligands were prepared for docking using Chimera (*31*) available at http://www.cgl.ucsf.edu/chimera/. All structural diagrams were prepared using VMD (*32*).

RESULTS

R108, S146, and D392 Are Involved in PLB1 Catalysis. Site-directed mutagenesis was used to generate the *C. neoformans* PLB1 substitutions R108A, S146A, and D392A (Figure 1). Each mutant cDNA was expressed in *S. cerevisiae* by growth in uracil-deficient/galactose-containing medium (URA$^-$ gal). *S. cerevisiae* was shown previously to be a

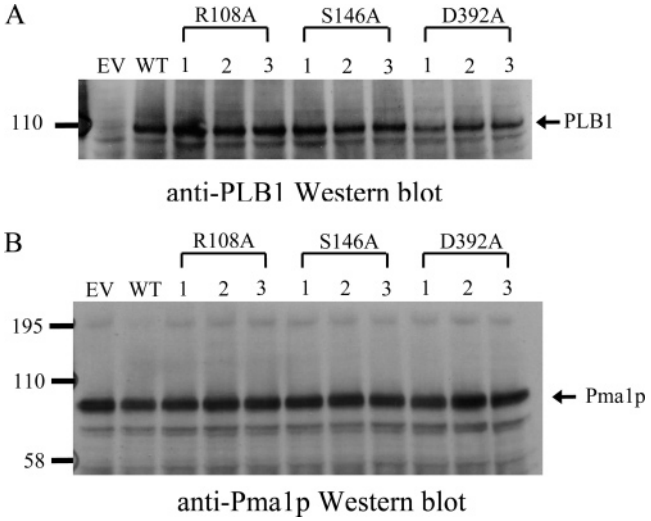

FIGURE 2: Detection of galactose-induced PLB1 expression. Lysates from three colonies of each *S. cerevisiae* transformant (indicated by 1, 2, and 3) that had been cultured in URA$^-$ gal medium to induce PLB1 expression were subjected to Western blotting with either the anti-PLB1 peptide antibody (panel A) or the anti-Pma1p antibody (panel B). The arrows indicate the positions of glycosylated PLB1 and Pma1p. 'EV' is the vector control.

suitable system for expressing cryptococcal PLB1, as the activity of recombinant PLB1 is similar to that of native PLB1 secreted from *C. neoformans* and significantly higher than that of endogenous PLB enzyme activity from *S. cerevisiae* (*2*, *21*).

Separate lysates were prepared from three colonies of each *S. cerevisiae* transformant and subjected to Western blotting with an anti-PLB1 peptide antibody (Figure 2A) and, as a control, an antibody against the endogenous membrane protein, Pma1p (Figure 2B). The intensity of the Pma1p band is similar in all lysates, indicative of equal protein loading across all samples. A 110 kDa band, present in the wild type but absent in the vector control and corresponding to fully glycosylated PLB1, was detected when gene expression was switched on by growth in URA$^-$ gal (*2*, *21*; Figure 2A). The band was absent when gene expression was switched off by growth in URA$^-$ glu (not shown). A band of similar size and intensity was observed for the three mutant PLB1s, indicating that all mutant PLB1 cDNAs were expressed at similar levels to wild type.

The effect of each mutation on cell-associated and secreted enzyme activities was assessed by radiometric assay (Table 1). Culture supernatants (secretions), cytosol/membrane (CM), and β-glucanase-treated insoluble (cell wall) fractions were prepared. Each mutation reduced LPL, LPTA, and PLB enzyme activities in all fractions to levels similar to or below the vector control (Table 1). In a control reaction performed previously using a primer without an introduced mutation (*21*), all activities were similar to wild type.

Homology Modeling of Cryptococcal PLB1. A BLAST search of the Brookhaven Protein Data Bank for PLB1 homologues revealed that PLB1 shares significant homology (17% identity) with human cPLA$_2\alpha$ (PLA2G4A), for which a 2.5 Å resolution atomic structure exists (PDB code 1CJY; *33*). Since PLB1 and cPLA$_2$ share the catalytic sequence motifs discussed above, we further investigated the homology between these proteins (Figure 1) to determine if the cPLA$_2$ structure could provide a suitable template for a homology

Table 1: Comparison of Secreted and Cell-Associated PLB1 Activities[a]

sample source	activity			total protein per fraction (mg)
	LPL	LPTA	PLB	
		Secreted		
vector only	1.21 (0.28)	1.01 (0.13)	0.09 (0.09)	0.16
WT	8.23[b] (0.73)	6.57[b] (0.60)	6.06[b] (0.25)	0.17
R108A	0.53 (0.05)	0.45 (0.03)	0.29 (0.14)	0.16
S146A	0.62 (0.10)	0.55 (0.06)	0.14 (0.14)	0.15
D392A	0.41 (0.05)	0.39 (0.05)	0.02 (0.02)	0.15
		CM		
vector only	0.73 (0.05)	0.28 (0.05)	0.72 (0.11)	1.31
WT	3.91[b] (0.40)	2.77[b] (0.30)	4.65[b] (0.12)	1.27
R108A	0.54 (0.10)	0.22 (0.05)	0.66 (0.06)	1.34
S146A	0.75 (0.08)	0.31 (0.04)	1.08 (0.06)	1.49
D392A	0.83 (0.18)	0.40 (0.11)	0.92 (0.06)	1.27
		Cell Wall		
vector only	1.54 (0.38)	0.80 (0.30)	6.62 (2.28)	0.13
WT	24.57[b] (0.63)	16.16[b] (0.91)	91.31[b] (12.85)	0.10
R108A	0.98 (0.44)	0.37 (0.30)	5.63 (1.03)	0.12
S146A	1.67 (0.89)	0.79 (0.73)	4.87 (0.75)	0.12
D392A	1.19 (0.56)	0.60 (0.34)	5.38 (0.87)	0.10

[a] *S. cerevisiae* transformants (cells and supernatants) were processed as described in Experimental Procedures to obtain the indicated fractions (CM is the cytosol/membrane fraction) and were assayed radiometrically for PLB1 activity also as described in Experimental Procedures. Data represent the mean and standard error where $n \geq 3$. Results are expressed as activity [μmol of lysoPC degraded or DPPC formed min^{-1} (mg of total protein)$^{-1}$ for LPL and LPTA, respectively, and nmol of DPPC degraded min^{-1} (mg of total protein)$^{-1}$ for PLB activity]. [b] Indicates that the increase in specific activity for the wild type is statistically significant compared with vector-only control and the mutants ($P < 0.001$). Differences between vector-only control and mutants were not statistically significant ($P > 0.05$). Statistical significance was determined using the Tukey−Kramer multiple comparisons test. The total protein (in milligrams) in the indicated fractions of each transformant is shown in the last column.

model of PLB1. Accurate predictions can be made with an amino acid sequence similarity greater than 50% between the target and the template protein, but even with very low homologies there may be considerable structural similarities, such as for the G-protein-coupled receptors and bacteriorhodopsin, where the sequence similarities within the transmembrane regions are only 6−11% (*34*). The conservation of the secondary structure elements is also relevant, since active sites and functional domains can have very similar geometries, even for distantly related proteins.

cPLA$_2$ is activated by intracellular calcium and preferentially cleaves substrates presented at a membrane interface, a phenomenon known as interfacial activation. cPLA$_2$ is comprised of two domains: an N-terminal C2 calcium binding domain (not represented) and a C-terminal catalytic domain (depicted in Figure 1). The catalytic domain is a unique fold related to, but distinct from, that of other lipases of the α/β hydrolase family. Its central core consists of a 10-stranded central mixed β-sheet surrounded by 9 α-helices (yellow rectangles). The cPLA$_2$ fold diverges from the canonical α/β hydrolase fold most significantly in containing a cap domain (cyan rectangles), part of which is thought to mediate interfacial activation by uncovering the active site when the protein engages the membrane. Among cPLA$_2$ isoforms, homology is concentrated in the α/β core while

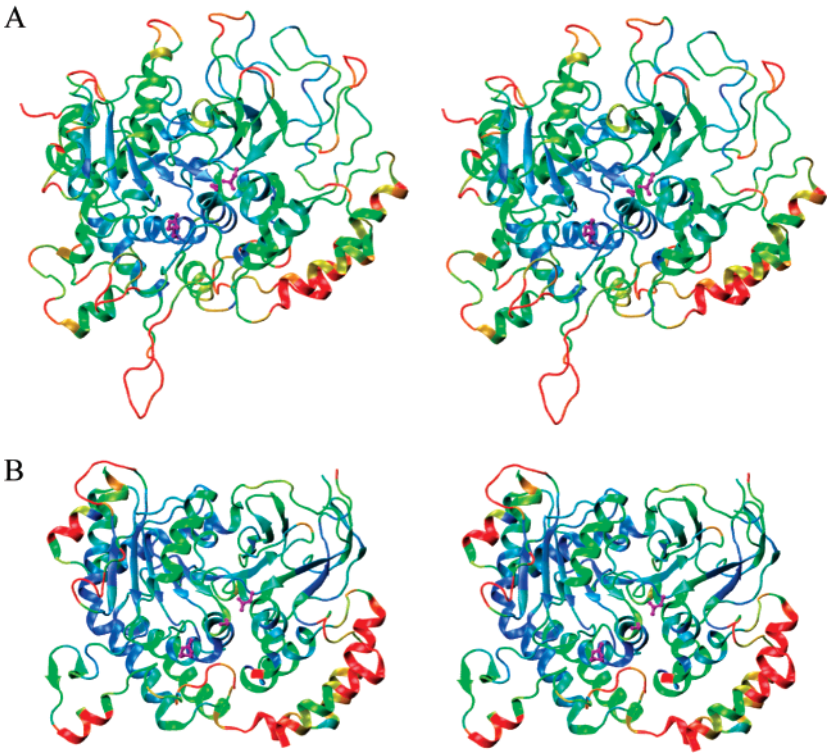

FIGURE 3: Stability of the PLB1 homology model. Stereo pairs of the structure of (A) the PLB1 homology model after 2 ns of unrestrained MD simulation and (B) the $cPLA_2$ catalytic domain. The protein is shown in cartoon form with β-strands depicted as arrows and α-helices as coiled ribbons, color-coded according to the rms deviation from the starting structure. The color scale for $cPLA_2$ is 0−3 Å and for PLB1 0−6 Å. The active site is approximately at the center of the figure, with (from bottom left) residues (PLB1/$cPLA_2$) R108/200, S146/228, and D392/549 shown in ball and stick form and colored purple.

the central part of the cap domain is distinct (*33*), suggesting that the cap may play a role in the substrate specificity of the protein.

The automated sequence search indicated that homology between PLB1 and the $cPLA_2$ catalytic domain existed only for the first half of PLB1, up to the C-terminal of α-helix fb (Figure 1) of the $cPLA_2$ cap domain (cyan region, Figure 1). This region of homology includes 7 of the 10 core β-strands of the $cPLA_2$ fold and their intervening α-helices, as well as the N-terminal two β-strands (β9a and β9b) and two α-helices (fa and fb) of the cap domain. Further manual alignment using the subtilisin protease aspartate motif as a reference point revealed significant homology in the C-terminal half of PLB1, completing homology for the remaining three β-strands of the $cPLA_2$ core and revealing good overall homology for the entire core β-sheet. In this alignment there is 21% identity and 50% similarity between the two sequences when measured as a percentage of the $cPLA_2\alpha$ sequence used for model building. In comparison, the sequence identity between the human serotonin transporter (SERT) and the crystal structure of the bacterial homologue from *Aquifex aeolicus* ($LeuT_{Aa}$) is about 20%, and several SERT models have been made using the $LeuT_{Aa}$ as a template (*35*, *36*). Thus we conclude there is good overall homology for the entire core β-sheet. This suggests that PLB1 and $cPLA_2$ are likely to share the same basic fold and that $cPLA_2$ is thus a suitable template for homology modeling of PLB1.

A homology model was generated using the software MODELLER. To further refine and test the model, we performed 2 ns unrestrained MD simulations of the protein in a water box. This helped to reveal incorrectly threaded sequences which were identified by their instability. As an aid to sequence threading, we also used the PHD neural network secondary structure and solvent accessibility prediction algorithm. In addition, N-linked glycosylation site occupancy was assigned only to solvent-exposed loops. It is predicted both from the N-linked glycosylation consensus sequences and from the high percentage of the PLB1 molecular weight (greater than 30%) that is attributable to N-linked glycosylation (*1*) that all 17 sites are occupied with sugar. Occupancy of two of these sites was confirmed by mass spectrometry (*21*; unpublished observation). They are N56 and N550 which are located at the N-terminus and just before αI, respectively. Sequence alignments were used to ensure that, where appropriate, the amphipathicity of helical regions was conserved across all known PLB isoforms. By an iterative process of sequence rethreading, model building, and MD simulations, we determined that the most stable model could be built if we presumed that PLB1 lacked the central, most divergent part of the cap domain which spans α-helix fb to α-helix fd in $cPLA_2$. In the $cPLA_2$ crystal structure, most of this region is disordered with the middle section forming a lid over the active site. This exercise also revealed that PLB1 diverges significantly C-terminal to αI, with an approximately 50-residue insertion between αI and αJ. The secondary structure predictions suggest that this region may form three β-strands, and this assignment is consistent with the location of two N-linked glycosylation sites, which occur on predicted turns between the β-strands.

Figure 3 illustrates the rms deviation of α-carbon residues from their starting positions after 2 ns MD simulations of $cPLA_2$ and the PLB1 homology model. For both structures, we observe that the central β-sheet and the α-helices which

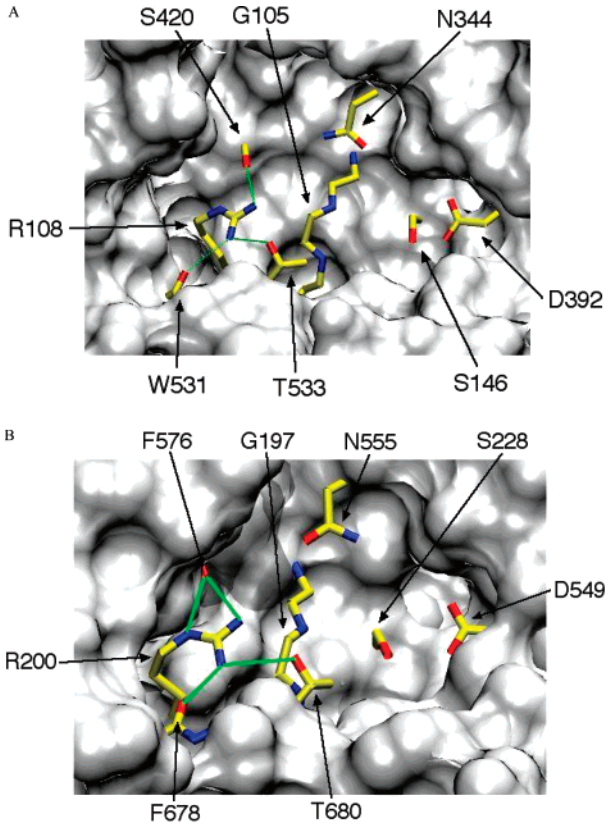

FIGURE 4: View of the active site clefts of homology-modeled PLB1 (panel A) and $cPLA_2$ (panel B) showing conserved residues. Labeled residues are shown in stick form and colored yellow (carbon), blue (nitrogen), and red (oxygen). Other residues are depicted as a surface representation using a probe radius of 1.4 Å. Hydrogen bonds are depicted as green lines. Panel A: PLB1 active site. Residues 421 and 422 have been removed to reveal the backbone carbonyl oxygen of S420 and the side chain of R108. Panel B: $cPLA_2$ active site. Cap domain residues 415−424 for $cPLA_2$, which partially occlude the active site in the X-ray structure (PDB code 1CYJ), have been removed for clarity. Residues 577 and 578 have been removed to reveal the backbone carbonyl oxygen of F576. The backbone nitrogen atoms of G105/G197 (labeled) and G106/G198 form a putative oxyanion hole, with S146/S228 and D392/D549 forming the catalytic dyad. R108/R200 is thought to bind the phosphate moiety of the lipid headgroup and may also stabilize the geometry of the oxyanion hole.

pack against it at the protein core are most stable. Loop regions and helices associated with the cap domain are more mobile in PLB1 (Figure 3B, upper right area). These data suggest that PLB1 and $cPLA_2$ are likely to share the same basic fold and that $cPLA_2$ is thus a suitable template for homology modeling of PLB1.

Schematic representations of the active site binding grooves of $cPLA_2$ and PLB1, as revealed by homology modeling, are shown in Figure 4. The homology modeling supports the idea that PLB1 is structurally and functionally closely related to the catalytic domain of human $cPLA_2$, sharing its core fold and varying predominantly in loop regions involved in substrate recognition and binding (Figure 1). The S146 and D392 residues are also in close enough proximity to function as a catalytic dyad. Thus, it would be expected that the two proteins share identical catalytic and interfacial activation mechanisms.

Ligand Binding to cPLA$_2$. Despite sharing the same catalytic site residues and hydrophobic active site groove, $cPLA_2$ removes only a single acyl chain at the *sn*-2 position, preferably arachidonic acid (but palmitic and oleic acids are also used), while PLB1 removes acyl chains from both the *sn*-1 and the *sn*-2 positions (preferably oleic and palmitic acids). In order to determine the likely binding mode of ligand to $cPLA_2$ and thus identify residues involved in the protein's substrate specificity, we used the program DOCK to model the interaction with lipid substrate.

Assessing the Binding of the Lipid Headgroup. An initial attempt to dock the lipid, 1-palmitoyl-2-oleoyl-*sn*-glycero-3-phosphatidylethanolamine, a lipid that was readily available for modeling, placed the phosphate group in contact with the active site arginine. However, while placing the *sn*-1 and *sn*-2 ester bonds proximal to the catalytic dyad, both bonds were hindered sterically from a catalytically productive interaction. It was thus decided to try to dock a lipid with 4-carbon acyl chains at the *sn*-1 and *sn*-2 positions, to increase the conformational sampling of the docking program. The top 100 conformers output by DOCK were examined to find those in which the *sn*-2 ester bond was suitably positioned for a nucleophilic attack by the active site serine. Only one conformer fulfilling this criterion was found. To refine the interaction of this conformer with the protein, we subjected the ligand−protein complex to a 0.5 ns MD simulation. The final structure after 500 steps of conjugate gradient minimization is shown in Figure 5, in which panel A illustrates the interaction of the lipid with the catalytic dyad and the putative oxyanion hole, which is formed by the backbone amide nitrogen atoms of G197 and G198. This structure shows clearly how the geometry and electrostatic complementarity of the modeled interaction are in complete concordance with the catalytic mechanism proposed by Dessen et al. (*33*).

Panel B of Figure 5 shows the interaction of the phosphate group with the conserved active site arginine and illustrates a possible role of a conserved asparagine (N555 in $cPLA_2$, N344 in PLB1) in binding the *sn*-1 ester oxygen. The equivalent asparagine is conserved in all three human $cPLA_2$ isoforms and, based on our alignment (Figure 1), in 52 of the 60 closest sequenced homologues of PLB1 as revealed by a BLAST search (data not shown). $cPLA_2$ S577, which binds the nitrogen of the lipid headgroup in the modeled interaction (Figure 5B), is found in two of the three human $cPLA_2$ isoforms; however, the equivalent residue is a serine (49 cases) or threonine (5 cases) in 54 of 60 PLB1 homologues. Since the interaction of the serine with the lipid headgroup nitrogen observed in the model would be formed more easily with the ethanolamine moiety than with the choline moiety, this suggests that the PLB1 isoforms may have a preference for phosphatidylethanolamines. The residue equivalent to T680, which binds to the conserved active site arginine side chain in the $cPLA_2$ structure, is not conserved either in human $cPLA_2$s or in PLB1 isoforms, suggesting that this interaction is not critical to the enzyme's function. The variability at this point is consistent with our modeling of the interaction of the protein with the lipid acyl chains, which indicates that this residue contacts the *sn*-2 acyl chain (see below).

Assessing the Binding of the Lipid Acyl Chains. To investigate possible binding modes of the lipid acyl chains, we independently docked palmitic acid and arachidonic acid to the $cPLA_2$ crystal structure. In each case, the first 100 conformers produced by the program were examined. Only

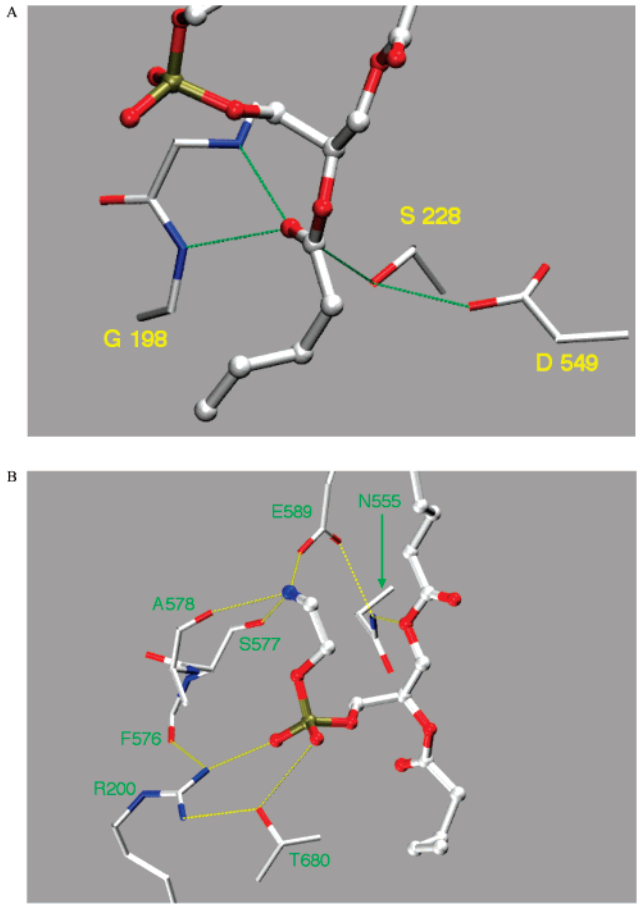

FIGURE 5: Binding of the lipid headgroup to the $cPLA_2$ active site. 1,2-Dibutyl-*sn*-glycero-3-phosphatidylethanolamine is shown in ball and stick form and protein atoms in stick form with oxygen colored red, carbon white, nitrogen blue, and phosphorus gold. Residues are as indicated. The figure comes from an energy-minimized structure of the enzyme−ligand complex after 0.5 ns of unrestrained MD simulation. Hydrogen bonds are shown as dotted lines, green in panel A and yellow in panel B. Panel A depicts ground state interaction of the region of the *sn*-2 ester bond with the catalytic dyad and oxyanion hole. In the mechanism proposed by Dessen et al. (*34*), D549 activates S228 by abstracting a proton during its nucleophilic attack at the *sn*-2 ester. An oxyanion hole formed by the backbone amide groups of G197 and G198 polarizes the *sn*-2 ester and stabilizes the transition state of the developing tetrahedral intermediate. The serine-acyl intermediate is generated upon collapse of the tetrahedral intermediate with transfer of a proton from D549 to the leaving lysophospholipid. Panel B depicts binding of the phosphatidylethanolamine moiety and the *sn*-1 ester oxygen to the $cPLA_2$ active site. Interaction of the phosphate group with the conserved active site arginine (R200) is indicated by hydrogen bonding, and a possible role of a conserved asparagine (N555) is indicated by the arrow. Residues are as indicated.

conformers in which the acyl chain did not sterically overlap the region occupied by the phosphatidylethanolamine moiety (see above), and in which one carboxyl oxygen coincided to within 0.5 Å with the appropriate ester oxygen of the docked 1,2-dibutyl-*sn*-glycero-3-phosphatidylethanolamine, were examined. For arachidonic acid, it was observed that the lower tract around the rim of the active site (Figure 6, red region) was the only region that was populated multiple times. This same tract also formed the binding site of the palmitoyl chain in the initial docking attempt using 1-palmitoyl-2-oleoyl-*sn*-glycero-3-phosphatidylethanolamine (see above). In this docking mode, the tail of the acyl chain curls around a cradle formed by a loop between helices H and I

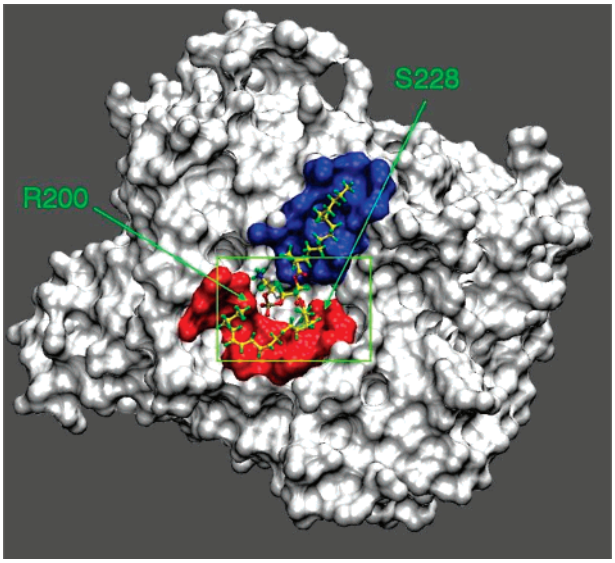

FIGURE 6: Binding of lipid fatty acyl chains to the $cPLA_2$ active site. Surface depiction of $cPLA_2$ using a 1.6 Å radius probe. A composite of 1-palmitoyl-2-arachidonoyl-*sn*-glycero-3-phosphatidylethanolamine is depicted in ball and stick form with carbon colored yellow, hydrogen green, oxygen red, nitrogen blue, and phosphorus gold. Residues which form the binding tracts for the arachidonoyl (*sn*-2) and palmitoyl (*sn*-1) chains are colored red and blue, respectively. The orientation of the molecule is the same as that depicted in Figure 4B with the region shown in Figure 4B delineated by a box (green). The locations of active site residues R200 and S228 are also indicated to aid orientation.

that is highly variable in sequence and length among both $cPLA_2$ isoforms and PLB1 (unfilled boxed region in Figure 1). Binding of the palmitoyl acyl chain was less variable and predominantly occurred in the mode illustrated in Figure 6 (upper tract; blue region), with variations in the configuration of the last four to six carbons of the tail. Thus our data identify different binding sites, specifically for palmitic acid and arachidonic acid substrates, and suggest that these regions may be at least partially involved in determining the substrate specificity of the protein.

DISCUSSION

PLB1 Has a Single Active Site That Utilizes a Serine−Aspartate Catalytic Dyad. Both the site-directed mutagenesis study and the homology modeling confirm the presence of a single PLB1 active site that catalyzes all three enzyme activities. This active site is composed of S146, D392, and R108, which are analogous to S228, D549, and R200 in $cPLA_2$ (*6*, *7*). The identical positioning of the three, shared catalytic residues within a similar hydrophobic binding funnel suggests the presence of a common catalytic mechanism with S146/228 and D392/549 situated in close enough proximity to function as a catalytic dyad and R108/R200 being sufficiently distanced to act as a stabilizer for the phospholipid headgroup. This idea is further supported by the lipid docking study, which confirms that the geometry and electrostatic complementarity of the modeled ligand−protein complex are consistent with these ideas. The hypervariability in the sequence comprising the lower binding tract, which accommodates the *sn*-2 acyl chain, may also explain the difference in acyl chain specificity between $cPLA_2$ and PLB1.

PLB1 Has Separate Binding Sites for the Lipid Acyl Chains. The finding from the docking study that each lipase

appears to have one substrate binding site composed of two separate binding tracts for the *sn*-1 and *sn*-2 acyl chains of the ligand provides an explanation for our previous studies demonstrating differential inhibition of either the LPL/LPTA or the PLB activities of secreted cryptococcal PLB1 by various acyl chain-containing agents (*1*, *3*, *19*, *20*). The differential effects of inhibitors on enzyme activity may be due to their preference for interaction with one or the other of the acyl chain binding tracts. An inhibitor that affects PLB but not LPL activity may sit only within the upper binding track where it would not sterically hinder the binding of a lysophospholipid, as the single acyl chain could still be accommodated within the lower binding tract, where catalytic cleavage occurs. Alternatively, it is also possible that the initial point of substrate contact with the enzyme may not be confined to the enzyme active site and may be different for phospholipids and lysophospholipids. The latter would explain why some inhibitors are specific for LPL and not PLB activity.

PLB1 Lacks the cPLA$_2$ Active Site Lid. The results of the homology modeling suggest that, while having regions corresponding to most of the cPLA$_2$ cap domain, PLB1 lacks the central lid that occludes the active site in the cPLA$_2$ structure. It has been suggested that the lid may be involved in interfacial activation. However, since PLB1 also displays interfacial activation but lacks the lid, our data argue against this interpretation. Since the lid region is hypervariable in sequence among cPLA$_2$ isoforms, and between cPLA$_2$ and PLB1 as demonstrated in this work, it may be involved in substrate specificity. Thus, an alternative explanation is that the lid recognizes the appropriate lipid membrane substrate and is thereby removed, allowing access to the active site. Alternatively, the action of the lid may be controlled by other proteins or possibly the C2 calcium binding domain.

In summary, we have shown that PLB1 contains a single active site for the catalysis of both phospholipids and lysophospholipids. Homology modeling suggests that PLB1 shares the same core fold as the cPLA$_2$ catalytic domain and, like cPLA$_2$, S146 and D392 form a catalytic dyad within a hydrophobic binding funnel, a feature which was previously thought to be specific for the cPLA$_2$ family of enzymes. Significantly, this model also suggests that PLB1 probably does not have a region equivalent to the central part of the cap domain, which occludes the cPLA$_2$ active site, suggesting that this lid region may be involved in regulation rather than interfacial activation. Finally, in silico modeling identifies potential binding sites for the lipid acyl chain within the lower tract of cPLA$_2$, where hydrolysis is predicted to occur, and through the homology model, also in PLB1, thus providing a structural basis for interpretation of the differences in substrate specificity between lipases sharing the cPLA$_2$ catalytic domain fold and for the differential effect of inhibitors on the various PLB1 enzymatic activities. The model also allows a prediction of the effects of mutations within PLB1 and thus represents a further step toward the rational design of agents to control PLB1 activity and function.

REFERENCES

1. Chen, S. C., Wright, L. C., Golding, J. C., and Sorrell, T. C. (2000) Purification and characterization of secretory phospholipase B, lysophospholipase and lysophospholipase/transacylase from a virulent strain of the pathogenic fungus *Cryptococcus neoformans*, *Biochem. J. 347*, 431−439.
2. Djordjevic, J. T., Del Poeta, M., Sorrell, T. C., Turner, K. M., and Wright, L. C. (2005) Secretion of cryptococcal phospholipase B1 (PLB1) is regulated by a glycosylphosphatidylinositol (GPI) anchor, *Biochem. J. 389*, 803−812.
3. Ganendren, R., Carter, E., Sorrell, T., Widmer, F., and Wright, L. (2006) Phospholipase B activity enhances adhesion of *Cryptococcus neoformans* to a human lung epithelial cell line, *Microbes Infect. 8*, 1006−1015.
4. Cox, G. M., McDade, H. C., Chen, S. C., Tucker, S. C., Gottfredsson, M., Wright, L. C., Sorrell, T. C., Leidich, S. D., Casadevall, A., Ghannoum, M. A., and Perfect, J. R. (2001) Extracellular phospholipase activity is a virulence factor for *Cryptococcus neoformans*, *Mol. Microbiol. 39*, 166−175.
5. Santangelo, R., Zoellner, H., Sorrell, T., Wilson, C., Donald, C., Djordjevic, J., Shounan, Y., and Wright, L. (2004) Role of extracellular phospholipases and mononuclear phagocytes in dissemination of cryptococcosis in a murine model, *Infect. Immun. 72*, 2229−2239.
6. Sharp, J. D., Pickard, R. T., Chiou, X. G., Manetta, J. V., Kovacevic, S., Miller, J. R., Varshavsky, A. D., Roberts, E. F., Strifler, B. A., and Brems, D. N. (1994) Serine 228 is essential for catalytic activities of 85-kDa cytosolic phospholipase A2, *J. Biol. Chem. 269*, 23250−23254.
7. Pickard, R. T., Chiou, X. G., Strifler, B. A., DeFelippis, M. R., Hyslop, P. A., Tebbe, A. L., Yee, Y. K., Reynolds, L. J., Dennis, E. A., Kramer, R. M., and Sharp, J. D. (1996) Identification of essential residues for the catalytic function of 85-kDa cytosolic phospholipase A$_2$, *J. Biol. Chem. 271*, 19225−19231.
8. Lee, K. S., Patton, J. L., Fido, M., Hines, L. K., Kohlwein, S. D., Paltauf, F., Henry, S. A., and Levin, D. E. (1994) The *Saccharomyces cerevisiae* PLB1 gene encodes a protein required for lysophospholipase and phospholipase B activity, *J. Biol. Chem. 269*, 19725−19730.
9. Merkel, O., Fido, M., Mayr, J. A., Pruger, H., Raab, F., Zandonella, G., Kohlwein, S. D., and Paltauf, F. (1999) Characterization and function *in vivo* of two novel phospholipases B/lysophospholipases from *Saccharomyces cerevisiae*, *J. Biol. Chem. 274*, 28121−28127.
10. Leidich, S. D., Ibrahim, A. S., Fu, Y., Koul, A., Jessup, C., Vitullo, J., Fonzi, W., Mirbod, F., Nakashima, S., Nozawa, Y., and Ghannoum, M. A. (1998) Cloning and disruption of *caPLB1*, a phospholipase B gene involved in the pathogenicity of *Candida albicans*, *J. Biol. Chem. 273*, 26078−26086.
11. Sugiyama, Y., Nakashima, S., Mirbod, F., Kanoh, H., Kitajima, Y., Ghannoum, M. A., and Nozawa, Y. (1999) Molecular cloning of a second phospholipase B gene, *caPLB2* from *Candida albicans*, *Med. Mycol. 37*, 61−67.
12. Oishi, H., Morimoto, T., Watanabe, Y., and Tamai, Y. (1999) Purification and characterization of phospholipase B from *Kluyveromyces lactis*, and cloning of phospholipase B gene, *Biosci., Biotechnol., Biochem. 63*, 83−90.
13. Masuda, N., Kitamura, N., and Saito, K. (1991) Primary structure of protein moiety of *Penicillium notatum* phospholipase B deduced from the cDNA, *Eur. J. Biochem. 202*, 783−787.
14. Watanabe, Y., Yashiki, Y., Sultana, G. N., Maruyama, M., Kangawa, K., and Tamai, Y. (1994) Cloning and sequencing of phospholipase B gene from the yeast *Torulaspora delbrueckii*, *FEMS Microbiol. Lett. 124*, 29−34.
15. Shen, D. K., Noodeh, A. D., Kazemi, A., Grillot, R., Robson, G., and Brugere, J. F. (2004) Characterisation and expression of phospholipases B from the opportunistic fungus *Aspergillus fumigatus*, *FEMS Microbiol. Lett. 239*, 87−93.
16. Yang, P., Du, H., Hoffman, C. S., and Marcus, S. (2003) The phospholipase B homolog *Plb1* is a mediator of osmotic stress response and of nutrient-dependent repression of sexual differentiation in the fission yeast *Schizosaccharomyces pombe*, *Mol. Genet. Genomics 269*, 116−125.
17. Huang, Z., Payette, P., Abdullah, K., Cromlish, W. A., and Kennedy, B. P. (1996) Functional identification of the active-site nucleophile of the human 85-kDa cytosolic phospholipase A$_2$, *Biochemistry (Moscow) 35*, 3712−3721.
18. Dessen, A. (2000) Structure and mechanism of human cytosolic phospholipase A$_2$, *Biochim. Biophys. Acta 1488*, 40−47.
19. Santangelo, R. T., Nouri-Sorkhabi, M. H., Sorrell, T. C., Cagney, M., Chen, S. C., Kuchel, P. W., and Wright, L. C. (1999) Biochemical and functional characterisation of secreted phospho-

lipase activities from *Cryptococcus neoformans* in their naturally occurring state, *J. Med. Microbiol. 48*, 731−740.
20. Ganendren, R., Widmer, F., Singhal, V., Wilson, C., Sorrell, T., and Wright, L. (2004) *In vitro* antifungal activities of inhibitors of phospholipases from the fungal pathogen *Cryptococcus neoformans*, *Antimicrob. Agents Chemother. 48*, 1561−1569.
21. Turner, K. M., Wright, L. C., Sorrell, T. C., and Djordjevic, J. T. (2006) N-linked glycosylation sites affect secretion of cryptococcal phospholipase B1, irrespective of glycosylphosphatidylinositol anchoring, *Biochim. Biophys. Acta 1760*, 1569−1579.
22. Thompson, J. D., Higgins, D. G., and Gibson, T. J. (1994) CLUSTAL W: improving the sensitivity of progressive multiple sequence alignment through sequence weighting, position-specific gap penalties and weight matrix choice, *Nucleic Acids Res. 22*, 4673−4680.
23. Sali, A., and Blundell, T. L. (1993) Comparative protein modelling by satisfaction of spatial restraints, *J. Mol. Biol. 234*, 779−815.
24. Rost, B., and Sander, C. (1993) Prediction of protein secondary structure at better than 70% accuracy, *J. Mol. Biol. 232*, 584−599.
25. Kalé, L., Skeel, R., Bhandarkar, M., Brunner, R., Gursoy, A., Krawetz, N., Phillips, J., Shinozaki, A., Varadarajan, K., and Schulten, K. (1999) NAMD2: Greater scalability for parallel molecular dynamics, *J. Comput. Phys. 151*, 283−312.
26. MacKerell, A. D., Jr., Bashford, D., Bellott, M., Dunbrack, R. L., Jr., Evanseck, J. D., Field, M. J., Fischer, S., Gao, J., Guo, H., Ha, S., Joseph-McCarthy, D., Kuchnir, L., Kuczera, K., Lau, F. T. K., Mattos, C., Michnick, S., Ngo, T., Nguyen, D. T., Prodhom, B., Reiher, I., W. B., Roux, B., Schlenkrich, M., Smith, J. C., Stote, R., Straub, J., Watanabe, M., Wiorkiewicz-Kuczera, J., Yin, D., and Karplus, M. (1998) All-atom empirical potential for molecular modeling and dynamics studies of proteins, *J. Phys. Chem. B 102*, 3586−3616.
27. Jorgensen, W. L., Chandrasekhar, J., Madura, J. D., Imprey, R. W., and Klein, M. L. (1983) Comparison of simple potential functions for simulating liquid water, *J. Chem. Phys. 79*, 926−935.
28. Ryckaert, J., Ciccotti, G., and Berendsen, H. (1977) Numerical integration of the cartesian equations of motion of a system with constraints: molecular dynamics of *n*-alkanes, *J. Comput. Phys. 23*, 327−341.
29. Darden, T. A., York, D. M., and Pedersen, L. G. (1993) Particle mesh Ewald: An $N\cdot\log(N)$ method for Ewald sums in large systems, *J. Chem. Phys. 98*, 10089−10092.
30. Schlick, T., Skeel, R. D., Brunger, A. T., Kalé, L. V., Hermans, J., Schulten, K., and Board, J. A., Jr. (1999) Algorithmic challenges in computational molecular biophysics, *J. Comput. Phys. 151*, 9−48.
31. Pettersen, E. F., Goddard, T. D., Huang, C. C., Couch, G. S., Greenblatt, D. M., Meng, E. C., and Ferrin, T. E. (2004) UCSF Chimera−A visualization system for exploratory research and analysis, *J. Comput. Chem. 25*, 1605−1612.
32. Humphrey, W., Dalke, A., and Schulten, K. (1996) VMD−Visual Molecular Dynamics, *J. Mol. Graphics 14*, 33−38.
33. Dessen, A., Tang, J., Schmidt, H., Stahl, M., Clark, J. D., Seehra, J., and Somers, W. S. (1999) Crystal structure of human cytosolic phospholipase A_2 reveals a novel topology and catalytic mechanism, *Cell 97*, 349−360.
34. Hibert, M. F., Trumpp-Kallmeyer, S., Bruinvels, A., and Hoflack, J. (1991) Three-dimensional models of neurotransmitter G-binding protein-coupled receptors. *Mol. Pharmacol. 40*, 8−15.
35. Ravna, A. W., Jaronczyk, M., and Sylte, I. (2006) A homology model of SERT based on the LeuT($_{Aa}$) template, *Bioorg. Med. Chem. Lett. 16*, 5594−5597.
36. Kaback, H. R., and Wu, J. (1997) From membrane to molecule to the third amino acid from the left with a membrane transport protein, *Q. Rev. Biophys. 30*, 333−364.

BI7009508